Third International Symposium on Marine Propulsors
smp'13, Launceston, Tasmania, Australia, May 2013

Full scale thruster performance and load determination based on numerical simulations

Norbert Bulten[1], Rik Suijkerbuijk[2]

[1]Wärtsilä Ship Power / Propulsion R&D, Drunen, The Netherlands
[2]Department of Mechanical engineering / Technical University Eindhoven, Eindhoven, The Netherlands

ABSTRACT

A method has been developed to determine full scale performance of steerable thrusters. The numerical simulations based on RANS-CFD have been validated with model scale measurements of various thruster geometries. Very good agreement between calculations and measurements has been found. The Reynolds scaling effect, which makes the difference between model scale and full scale calculations, has been analyzed and the occurring phenomena have been explained. Based on this a generic full scale thruster bollard pull performance method has been derived. Transient loads on the propeller shaft have been determined for straight sailing and for conditions with oblique inflow. The blade passing amplitudes of propeller thrust and torque, as well as the thruster steering torque have been analyzed. Amplitudes are below 10% for thrust and torque. Review of the steering torque has shown that both thrust eccentricity and a side force on the nozzle contribute to the final steering torque. These two phenomena are balancing each other to a certain extend.

Keywords

Numerical simulations (RANS-CFD), viscous flow, steerable thrusters, transient behavior

1 INTRODUCTION

Numerical flow simulations have been introduced within (the predecessor of) Wärtsilä Propulsion about 15 years ago. From the beginning on the types of analyses have been expanding. This was possible due to both the internal drive to make use of the numerical simulations and the external ongoing development of hardware and software. Another even more important development, which has contributed to the successful expansion of simulations, is the acceptance of the sometimes conservative shipbuilding industry. Nowadays, the results of CFD calculations are reviewed with less suspicion compared to a decade ago. This can be related to the improved accuracy of the calculations. However, another important step to get confidence in the numerical results is made once the numerical results can be explained based on (fairly) simple fluid dynamic theories. Once the occurring flow phenomena can be explained, the discussions on the applied meshes, turbulence modeling etc will become less important.

Understanding of the flow phenomena can be obtained by proper post-processing of the calculations, where the user should look further than thrust and torque of the unit only. The numerical methods are well-suited to divide the thruster-unit into different pieces to investigate the forces and moments, which act on these parts. In addition to this, it is straight forward to determine the flow rate through a thruster-unit. Once the flow rate is known for a thruster-unit, all available theory on axial pumps can be used to understand and explain the observed phenomena. Because of the difficulty to measure flow rates in a model test set-up of a thruster, it has not received proper attention from experimental side in the past.

Although there are clear limitations on model testing, it should be clear that there is still large interest in model scale testing. Testing of new thruster designs and new concepts, like tilted thruster units, can be done to prove that the designed thruster works as expected. In order to obtain proper validation material for CFD calculations, model testing is required as well. The importance of proper validation in the development of numerical methods can never be overestimated.

CFD analyses of thrusters have started at Wärtsilä around 2006. Results of the first steps of the method development process have been presented at various conferences. Typical phenomena which have been addressed were (i) the force and drag contributions of the different thruster components (propeller, nozzle, housing) for different operating conditions (Bulten, 2006) and (ii) the type of numerical simulation to be conducted to get proper results. Evaluation of the validity of quasi-steady and fully transient methods has been discussed (Bulten, 2008).

Implementation of a cavitation model in the CFD-RANS calculation of a tunnel thruster has been presented as well (Oprea & Bulten, 2011).

The developed numerical methods have been used in the design process of new Wärtsilä thrusters the last years. CFD has not only been used in the phase where the detailed performance is determined, but already in the phase of conceptual designs. In the concept phase CFD was used in a direct way for design evaluation. The indirect use of CFD has been even more important in this phase. Indirect use means the utilization of the accumulated knowledge of the occurring flow phenomena in a thruster-unit based on previous CFD analyses. Based on this understanding clear choices in the concept phase could be made, which have led to a well performing new thruster design.

In this paper, a clear distinction is made between load determination and performance determination. This is related to the use of the results in the design process. The loads are used internally to determine the structural integrity of the units. In such analysis normal engineering safety factors are included. Therefore the CFD analyses aim at finding the worst case scenarios and understanding the different loading conditions. Performance determination is based on well defined conditions (bollard pull and/or free sailing) for given input power. In these analyses the accuracy should be very high.

In the following sections of the paper the development of the numerical method will be discussed in more detail. The next section will deal with the performance determination based on CFD and the interpretation of the numerical results. As a follow-up of the ducted-propeller loss-coefficient method presented at SMP'11 (Bulten & Nijland, 2011), a generic performance method for thrusters has been developed.

In the subsequent two sections the results of transient analysis will be discussed. The focus will be on the transient shaft loads and on the hydrodynamics forces which create the thruster steering torque.

2 DEVELOPMENT OF NUMERICAL SIMULATIONS FOR THRUSTERS

2.1 Implementation of RANS method

It has been decided to use a Reynolds Averaged Navier-Stokes (RANS)-method for the numerical analyses. The motivation to select a RANS method is based on the achievable accuracy of the method, both on model scale and full scale. Typical flow phenomena like the flow through the clearance between propeller tip and nozzle and the flow at the trailing edge of the nozzle have to be captured well to get a proper solution. This disqualifies the potential flow based methods and panel methods, though it is known that these methods require significantly less computational resources and/or time compared to RANS.

The strategy with respect to meshing and numerical models is based on accurate extrusion layers near the surfaces of the thruster and the propeller. In this way a high quality mesh is made to capture the development of the boundary layer well. In order to keep the number of cells within acceptable limits, wall functions are used in the cell adjacent to the walls. In this approach y+ values of 200-300 are still allowed, whilst keeping good accuracy. In the remainder of the numerical domain a structured hexagonal mesh is used with refinements near the regions of interest. At typical thruster mesh can be build with 3-5 million cells with this approach. Computation times for quasi-steady performance calculations are within 1 hour on a computer cluster with 30 cores. For transient calculations the cell count has been reduced further to about 1.5 million cells. The general flow features can still be captured well with this coarser mesh. An example of the mesh, which has been made with Star-CCM+, is shown in figure 1, where the extrusion layer as well as the hexagonal background mesh can be recognized clearly. The 1-to-2 mesh refinement towards the unit is visible as well.

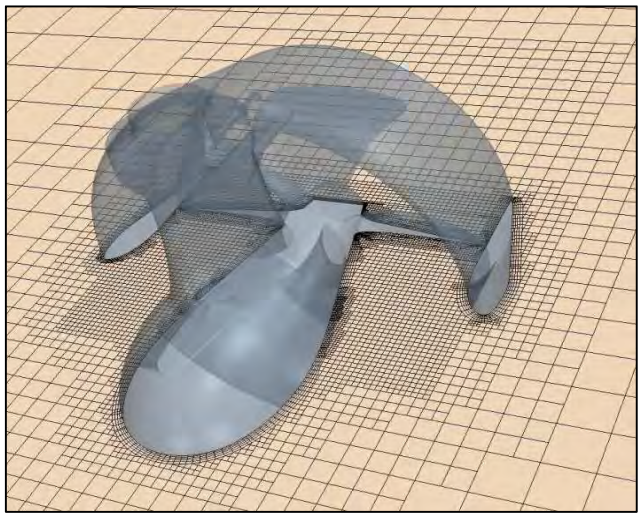

Figure 1: thruster mesh visualization in horizontal plane

2.2 Validation of method

The numerical method has been validated with aid of available experimental data. Three different thruster-configurations have been measured in open water set-up at Marintek in Norway. The typical characteristics of the units are shown in the table below. In order to get a sufficient high Reynolds number the propellers were made with a diameter of 250 mm at model scale and tests were run in the range of 10.8 to 16 rps. Forces were measured at the propeller shaft (propeller thrust and torque) and at the top of the unit (total thrust and side forces and steering torque).

Table 1: tested thruster configurations

Unit	Power	Full-scale Diameter	Nozzle-tilt
1	5500 kW	3.9 m	Straight
2	4500 kW	3.9 m	Straight
3	5500 kW	3.9 m	8-degree tilt

The results of the propeller thrust and torque as well as the complete unit thrust are used for comparison with model scale CFD calculations.

For one of the configurations, tests have been carried out with oblique inflow. In these tests the unit was given a fixed forward speed and propeller RPM. The orientation of the steerable thruster was changed from straight course (0 degrees) up to 60 degrees steering angle. In order to investigate the possible effects of the turning direction of the propeller (clockwise or counter-clockwise) also tests were done towards the negative steering direction (-60 degrees).

2.3 Validity of different numerical approaches

When setting-up a numerical method, one of the important decisions is whether the right solution can be obtained with a quasi-steady solution method based on moving-frame-of-reference (MFR) or if a fully transient calculation with moving mesh (MM) is required. Given the large difference in required computing power, it would be a waste, if MFR-methods are discarded from the beginning. On the other hand, there is always the risk that MFR-methods are used beyond their validity, since there will be always an outcome of the calculation in general. So, there are certain pitfalls to be considered, like analysis of thruster steering torque and lateral shaft forces (Bulten, 2008).

3 PERFORMANCE DETERMINATION

The thruster performance determination will focus both on bollard pull performance and free sailing performance. For the bollard pull performance the merit-coefficient will be used, whereas the normal propulsive efficiency is used for free sailing performance evaluation. The definition of both parameters will be shown below for clarity:

$$MC \equiv \frac{(K_{tt}/\pi)^{3/2}}{K_q} \qquad (1)$$

$$\eta = \frac{J \cdot K_{tt}}{2\pi \cdot K_q} \qquad (2)$$

In these equations the total unit thrust is represented by the dimensionless coefficient K_{tt} and the torque by K_q. The advance speed is represented with J.

3.1 Model scale performance

The results of one of the tested units are shown in figure 2. For the thruster-unit the total unit thrust is shown, as well as the propeller thrust and torque. Unit efficiency is calculated according equation (2). The agreement between model scale experimental data and model scale CFD data for thrust and torque is quite good over the range of operating conditions from bollard pull to the free sailing condition. The agreement for the open water efficiency is very good over the whole range.

Similar trends of good agreement have been found for the other tested configurations.

3.2 Full scale performance

In figure 3, the CFD results of calculations on model scale (propeller diameter of 0.25 m) and full scale (diameter of 3.9 m) are shown. A clear difference in efficiency is found between the two variants. The differences in propeller thrust and torque are not so pronounced in this comparison. This trend of significant performance increase due to Reynolds scaling effects is in line with the presented phenomena on ducted propellers (Bulten & Nijland, 2011).

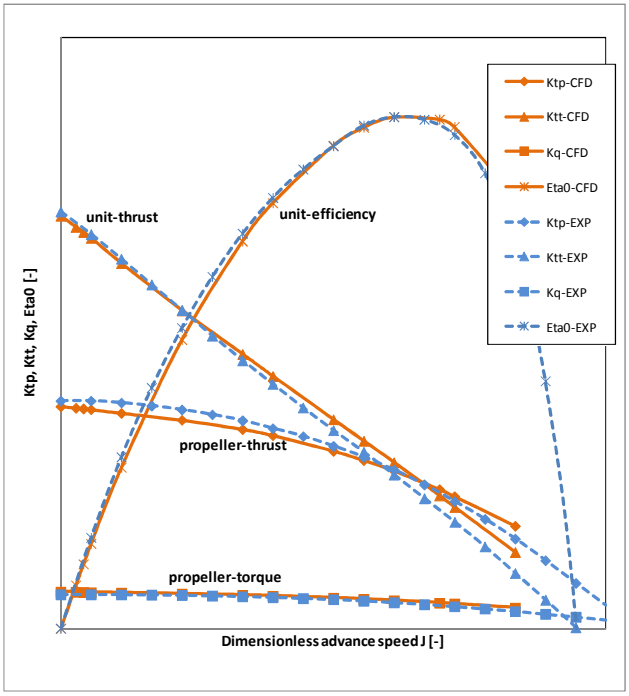

Figure 2: comparison model scale experimental data with model scale CFD results for thruster open water performance

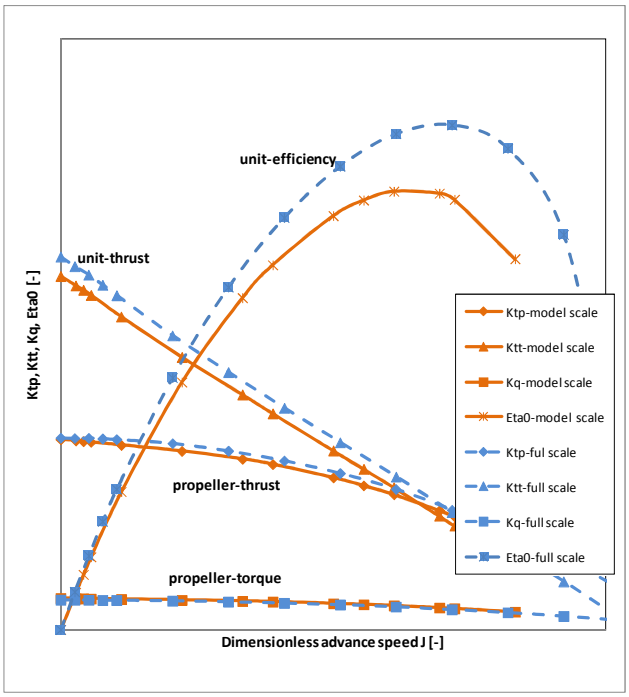

Figure 3: comparison of model scale and full scale CFD results for thruster open water performance

The bollard pull performance of the unit is expressed in the merit-coefficient as defined in equation (1). For the model scale case a merit coefficient of 1.31 is found, whereas the full scale merit is 1.50 for this unit. For equal power this means a difference of about 10% in bollard pull thrust.

3.3 Generic bollard pull performance prediction method

The method to determine bollard pull for ducted propellers has been discussed in detail in the paper of SMP'11. This method can be applied to ducted thruster-units as well.

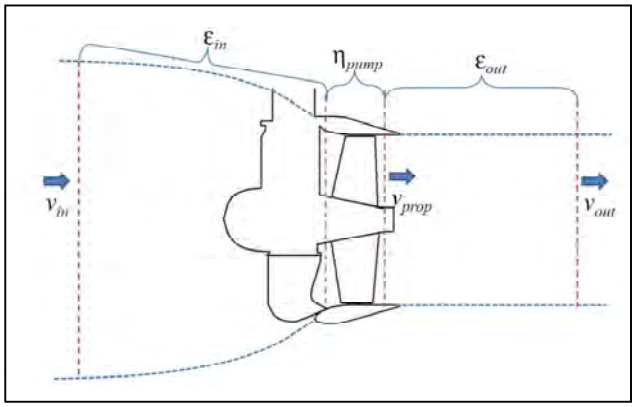

Figure 4: sketch of thruster-unit with merit-coefficient parameters

One of the important equations in this method is the expression for the merit coefficient based on the pump efficiency η_p, the outlet velocity ratio λ, defined as v_{prop}/v_{out} and the loss-coefficients ε_{in} and ε_{out}.

$$MC\big|_{j=0} = \frac{2 \cdot \sqrt{\lambda} \cdot \eta_p}{1 + \lambda^2(\varepsilon_{in} + \varepsilon_{out})} \qquad (3)$$

For full scale a pump-efficiency of 89-90% is found for a well designed fixed pitch propeller. For the model scale propeller the efficiency drops to 84%, which is very well in line with literature on pumps (Pfleiderer, 1961).

For the current reviewed thruster unit the outlet velocity factor is equal to 1.0 based on the design of the thruster nozzle. Although it has been stated before that a outlet velocity ratio λ larger than 1.0 is beneficial for bollard pull, this is only true for configurations with limited losses. Typical examples are shaft-driven controllable pitch propellers. In case of thruster-units the loss-coefficients increase due to the presence of the shank just upstream of the propeller. The additional losses due to this shank result in another optimal outlet velocity ratio.

Now the merit coefficient, the pump efficiency and the outlet velocity ratio have been determined. The inlet and exit loss coefficients can be derived from the CFD results or they can be derived from equation (3), since all other factors are known. The derived loss-coefficients are shown in Table 2, as well as the other parameters.

Table 2: thruster merit coefficients for full scale and model scale

	Pump efficiency	Loss-coefficient	Outlet velocity ratio λ	Merit coefficient
Full scale	0.89	0.190	1.0	1.50
Model scale	0.84	0.285	1.0	1.31

The difference in performance between model scale and full scale is related to the difference in pump efficiency, which has been addressed, and the difference in loss-coefficients. This difference can partly be attributed to the difference in frictional losses. The same phenomenon occurs in model scale hull resistance and self-propulsion testing. It has been acknowledged that the full scale wall friction is lower than the experienced model scale friction. Roughly speaking, the full scale wall friction factor is about half of the model scale factor. In order to take the reduced wall friction into account in a self-propulsion test, an additional pulling force is introduced, denoted as F_D (ITTC, 1978).

The loss-coefficients as found for the thruster units can be split into a viscous part and a non-viscous part.

$$\varepsilon_{in} + \varepsilon_{out} = \varepsilon_{tot} = \varepsilon_{viscous} + \varepsilon_{non-viscous} \qquad (4)$$

The following contributions can be derived for the loss coefficient components, based on the results for model scale and full scale and the difference in wall friction coefficient between model scale and full scale. The components of the loss-coefficient based on equation (4) are shown in table 3.

Table 3: thruster loss coefficients for full scale and model scale

	Total Loss-coefficient	Viscous component	Non-viscous component
Full scale	0.190	0.095	0.095
Model scale	0.285	0.190	0.095

Based on the values in tables 2 and 3 a good estimate can be made of the maximum achievable merit coefficient of a thruster unit. A total loss coefficient in the range 0.18-0.20 seems to be realistic, since it takes the viscous losses into account and the pressure drag on the shank and the gearbox of the unit. A realistically achievable axial pump efficiency is 90%. The outlet velocity ratio is 1.0 for this specific nozzle. Based on these values the maximum merit coefficient of 1.54 for an azimuthing thruster unit can be calculated.

3.4 Comparison to general rule of thumb for bollard pull performance prediction

A general rule of thumb for bollard pull performance prediction for steerable thrusters can be found in guidelines of IMCA for DP capability plots (IMCA, 2000). In this guideline it is stated that the expected thruster efficiency is about T/P=13 kg/hp. In SI quantities this is written as:

$$\frac{T}{P} = 0.18\left[\frac{kN}{kW}\right] \tag{5}$$

This general guideline can be compared to the generic merit-coefficient approach based on the following formula:

$$\frac{T}{P} = \sqrt[3]{\frac{\rho \cdot MC^2}{\left(P \Big/ \frac{\pi}{4} D^2\right)}} \tag{6}$$

Evaluation of this formula learns that not only the merit-coefficient, but also the power density of the unit (P/D^2) plays a role in the ratio of T/P. Both terms are not used in the generic guidelines. Evaluation of the guideline for different merit coefficients and power densities will show the accuracy of the generic rule.

Figure 5 shows the full scale thruster performance for a range of powers.

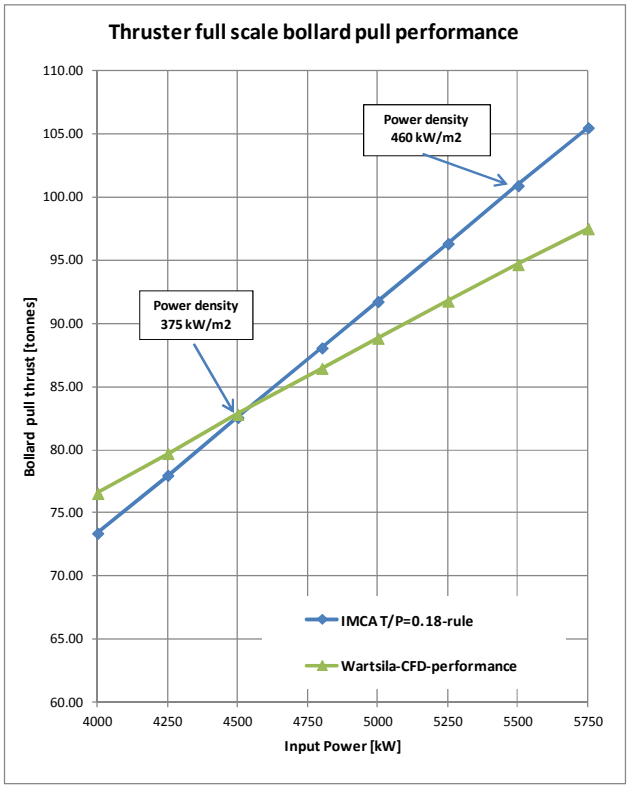

Figure 5: thruster bollard pull comparison based on equations (5) and (6)

At a low power density (around 375 kW/m^2) a very good match is found between the two formulas. However, the differences arise at higher power densities. At 460 kW/m^2 the difference is about 7% in bollard pull performance. This is not bad, given the simplicity of equation (5). For accurate thruster performance prediction equation (6) should be used however.

3.5 Example cases for bollard pull performance prediction

The theory presented above is showing mainly dimensionless numbers, efficiencies and loss-coefficients. In order to make it more practical two example cases are presented. First a comparison is made between a ducted propeller and a thruster unit and second the effect of increasing propeller diameter is shown. Results of both example cases are shown in figure 6. The target thrust is set to 94.5 ton bollard pull.

3.5.1 Example case 1: comparison ducted propeller with thruster unit

The effect of the shank and the thruster gearbox upstream of the propeller has been mentioned before. As a result the total loss-coefficient increases from 0.10 to about 0.19. In this case study the actual bollard pull thrust is calculated for a propeller with a 3.9 meter diameter. The ducted propeller performance is based on the HR-nozzle geometry, which has a maximum merit-coefficient of 1.72. The thruster performance is based on the LMT3510-thruster unit with WTN-nozzle, which has been designed specific for thruster applications. The LMT3510-thruster is designed to deliver 94.5 ton bollard pull at 5500 kW. It can be seen that this thrust is reached at much lower power setting for the ducted propeller case. For the ducted propeller about 4825 kW is needed.

3.5.2 Example case 2: Effect of propeller diameter

The influence of the propeller diameter is reflected in the power density (P/D^2). The power density will decrease when the propeller diameter is increased for given power. Based on equation (5), this will have a positive effect on the bollard pull thrust. In order to reach the same target thrust for a 4.1 meter propeller the required power is about 5225 kW. The reduction in power of about 5% is more or less in relation to the increase in diameter of 5% (4.1/3.9).

Based on the example cases it can be shown what the maximum realistic bollard pull performance of an azimuthing thruster will be. As mentioned before, the IMCA rule of T/P=0.18 give too optimistic values in the range above 5000 kW.

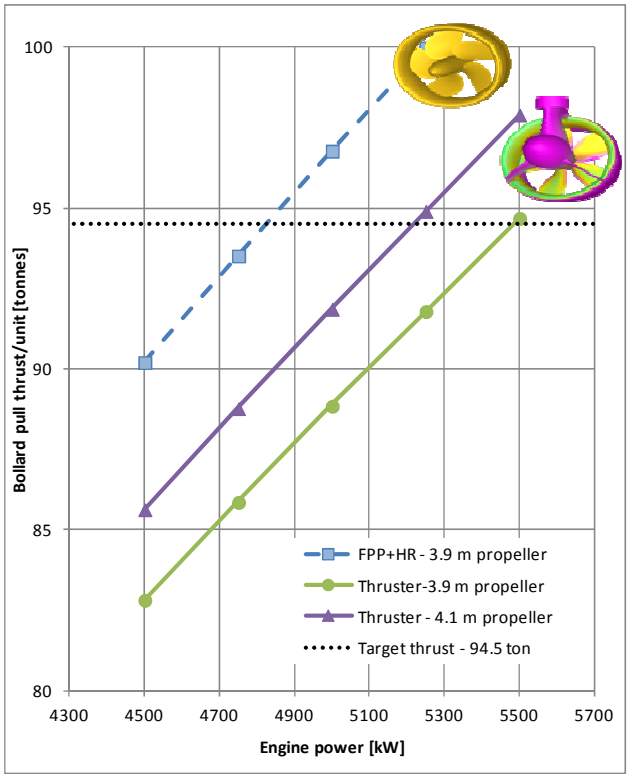

Figure 6: bollard pull performance prediction for 2 example case studies to analyze effect of thruster house geometry and propeller diameter variation

4 TRANSIENT SHAFT-LOAD DETERMINATION

In the previous section the thruster performance in bollard pull and free sailing condition has been reviewed. These performance figures are based on the time-averaged forces and moments. The actual loads on the propeller vary during a revolution due to the interaction effects with the shank and the brackets upstream of the propeller. These force fluctuations can be determined from the fully transient CFD calculations, based on the moving mesh approach. In this section the time-dependent, blade harmonic results will be analyzed in more detail.

First the operating conditions with straight inflow will be reviewed. The focus in the analysis is on the fluctuating propeller shaft thrust and torque, since these fluctuations are needed in the structural analysis of the unit.

Afterwards some conditions with oblique inflow will be analyzed. These calculations require the fully-transient moving mesh option to be in good agreement with experimental data. Results for one of the measured conditions will be shown.

The behavior of a steerable thruster without nozzle has been presented before by others (Amini *et al*, 2012). In the current research only ducted units will be reviewed. A detailed comparison between the observed phenomena for open and ducted propellers is not in the scope of this paper. It should be clear however, that the results for ducted propellers cannot be applied to thrusters with open propellers as well.

4.1 Shaft load fluctuations for straight inflow

The time-dependent harmonic CFD results of propeller thrust and torque have been fitted with a Fourier-series up to the 4th-blade harmonic:

$$T = \sum_{n=0}^{4} A_n \sin(n\omega t + \theta_n) \qquad (7)$$

The normalized amplitudes of fluctuations in propeller thrust and torque are shown in figure 7.

The normalized amplitude of the thrust and torque in free sailing condition is larger than the normalized amplitude in bollard pull condition. Detailed analysis of the actual results showed that this trend is also present in the values before normalizing. Based on this finding it can be concluded that the shank has more influence on the flow in the free sailing condition. The fluctuations in thrust values are in this case up to 6%. It has to be noted however that these calculations have not included cavitation effects. This will be one of the next steps in the research program.

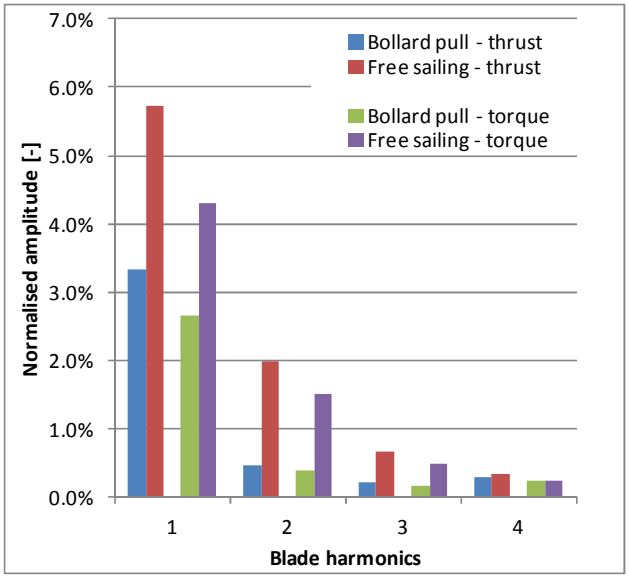

Figure 7: normalized amplitudes of propeller thrust and torque for bollard pull and free sailing condition

4.2 Comparison with measurements for conditions with oblique inflow

The calculations with oblique inflow have been performed with a fully transient moving mesh method. Four different conditions have been measured, where 2 different forward speeds of the carriage and 2 different propeller RPMs were used. This gave a matrix of 4 different conditions to be used for comparison with CFD results.

In figure 8 the CFD results for propeller thrust and torque as well as the unit thrust and side force are compared with experimental data. Agreement between CFD calculations and model scale measurements is good over the whole range of inflow angles.

A more detailed review of the results shows that there is a certain asymmetry between positive and negative steering angles. This is attributed to the effect of the propeller

rotation direction in combination with the obstruction of the thruster housing upstream in the flow.

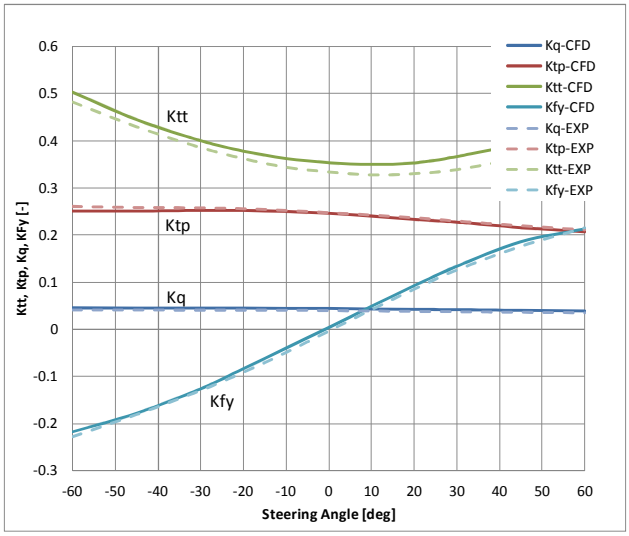

Figure 8: comparison of CFD results (solid lines) and experimental data (dotted lines) for unit thrust (Ktt), side force (Kfy), propeller thrust (Ktp) and torque (Kq) for a thruster-unit operated at different oblique inflow angles

4.3 Mean shaft loads for oblique inflow

The loads on the propeller shaft (thrust and torque) will be analyzed in more detail to study the effects of oblique inflow. One typical condition at free sailing condition has been selected for comparison. The inflow has been varied to -30 and +30 degrees. The mean values are plotted in the open water diagram for this thruster unit in Figure 9.

The results for the two cases with oblique inflow show several interesting phenomena. First of all the values either increase or decrease based on the direction of the inflow. Second the deviation from the straight inflow condition is not symmetrical. So, there seem to be different phenomena which play a role in the loading of the propeller. One of the phenomena is the change in flow rate through the nozzle. This leads to a shift in the operational point. In case of increased flow rate, an apparent increase of advance speed is found, which means decreased thrust and torque. A second effect which plays a role in the change is the presence of pre-swirl in the flow just upstream of the propeller. If the pre-swirl is in the same direction as the propeller rotation, then an apparent deduction of propeller RPM is found.

4.4 Shaft load fluctuations for oblique inflow

The analysis of the amplitude of the time-dependent fluctuations has been made for the conditions with oblique inflow as well. The amplitudes have been derived based on equation (7). Results are presented in figure 10. The asymmetry in the mean values for propeller thrust and torque has been discussed in the previous subsection.

The same trend can be observed when the amplitude of fluctuations in thrust and torque are reviewed. For negative inflow angles the amplitudes are significantly larger than for the straight inflow and the positive inflow angle. The trends for the propeller thrust and torque are more or less the same, which is in line with expectations.

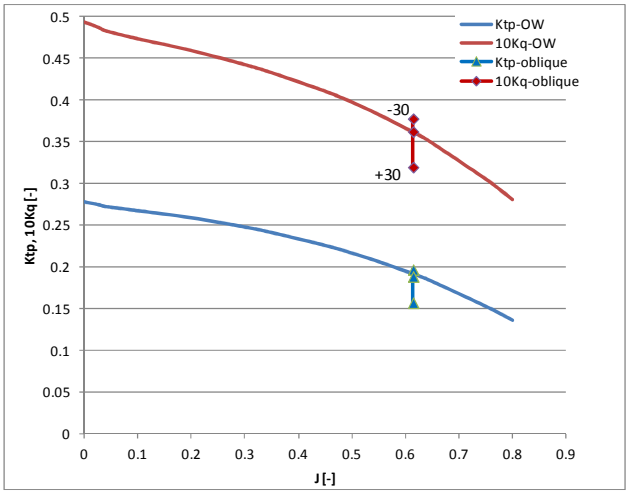

Figure 9: propeller thrust (Ktp) and torque (10Kq) in open water conditions and with oblique inflow

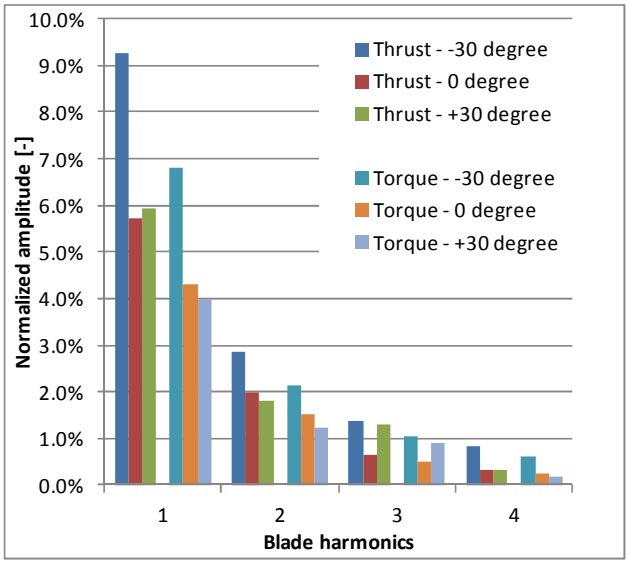

Figure 10: normalized amplitudes of propeller thrust and torque for free sailing with straight and oblique inflow

5 HYDRODYNAMIC STEERING TORQUE

The loads on the propeller shaft due to oblique inflow have been discussed in the previous section. The fully transient calculations with oblique inflow can be used as well to analyze the hydrodynamic steering torque on the unit.

5.1 Underlying physical phenomena

The analysis of the hydrodynamic steering torque can focus on the torque as a function of the inflow angle and the ship speed. This approach would be in line with an experimental set-up, where the steering torque on top of the unit is measured.

The numerical simulations give two other interesting options for analysis of the steering torque. First, the contribution of the different components (propeller, nozzle, gearbox) to the total torque can be identified. Second, the two components, which contribute to the total

torque, can be determined separately. The formula for the total torque is:

$$M_z = F_x \cdot y - F_y \cdot x \qquad (8)$$

In this equation F_x is the thrust eccentricity and F_y is the side force. Figure 11 shows a sketch of the two forces. The location of the forces in this sketch already indicate that both forces will balance the total steering torque to a certain extend in case of a pushing ducted thruster unit.

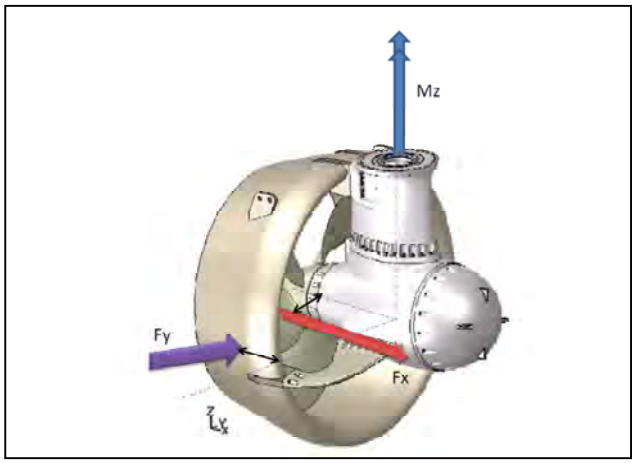

Figure 11: sketch of thruster with contributing forces to hydrodynamic steering torque

5.2 Evaluation of numerical results

The calculated pressure distribution on the thruster unit is shown in Figure 12 for the 0 degree steering, thus straight inflow, condition and the -30 degree steering condition for an advance speed of J=0.46. The pressure distribution on the nozzle and shank shows a clear difference, whereas the pressure distribution on the blades is quite the same for the two analyzed conditions. The pressure distribution on the nozzle at -30 degree oblique inflow shows a clear difference between both sides, which indicates a certain thrust eccentricity of the nozzle thrust. The eccentricity at this J-value will contribute to the steering torque.

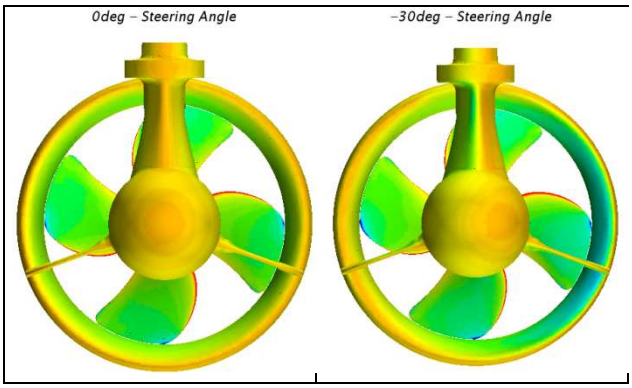

Figure 12: pressure distribution on thruster unit for 0 degree steering (left) and -30 degree steering

The calculated steering torque has been compared to the available experimental data. In Figure 13, the results are shown for 4 different advance speeds (J) and for 3 steering angles. Based on the results, it can be concluded that there is a deviation between the measurements and the CFD calculations. Interpretation of the cause of this deviation, based on this chart only is not straight forward. Either there is a shift in advance speed, or in the actual value of the steering torque. The overall trend is captured quite well with the numerical simulations.

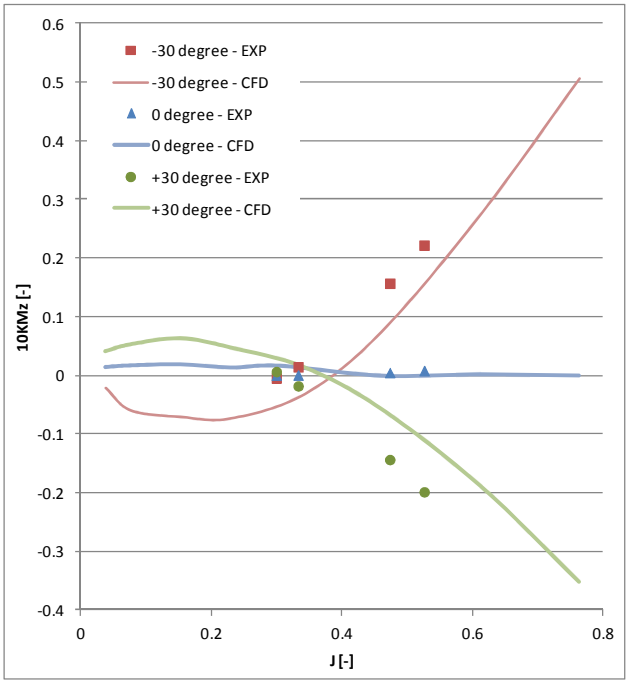

Figure 13: comparison model scale experimental data with model scale CFD results for thruster hydrodynamic steering torque

First a more detailed analysis of the actual trend of the steering torque is made. The overall steering torque changes sign when comparing operating conditions below and above J=0.3. This indicates that the two different components of the steering torque play both a role. At high speeds it is most likely that the side force becomes dominant over the thrust eccentricity. This explains the more or less quadratic increase at high J values. At lower advance speeds, the thrust of the propeller and the nozzle are much larger compared to high speeds, and as a result the thrust eccentricity contribution is larger. The influence of the side force is related to the value of the advance speed. Towards bollard pull (J=0) the three conditions seem to converge to the same value. This is in line with expectations, since towards bollard pull there is no (dependency of) inflow direction anymore.

Since both the thrust eccentricity and the side force play an important role, it is interesting to review the separate contributions to the total steering torque. Figure 14 shows the steering torque components as shown in equation (8) for two inflow angles. It can be seen that that both contributing components have a value of almost equal magnitude. The resulting steering torque is the difference between these two, and therefore it has become a relative small value, which is sensitive to small errors in the contributing components.

The contribution of the thrust eccentricity increases up to an advance ratio of about 0.3 and then slowly decreases again. This can be related to the decreasing propeller thrust with increasing advance speed. Up to moderate advance speeds the eccentricity will increase, which

results in increasing contribution to the torque. The contribution of the side force to the steering torque shows a linear increase. At first sight a quadratic curve would be expected, based on a force related to a constant drag coefficient and the squared inflow velocity. In this case it is not applicable, since both the drag coefficient and the velocity components change due to steering.

Fairly small differences in one or both of the components can easily lead to relative large differences in the total torque. Given this fact, the deviation between the measurements and the numerical simulation, can be explained.

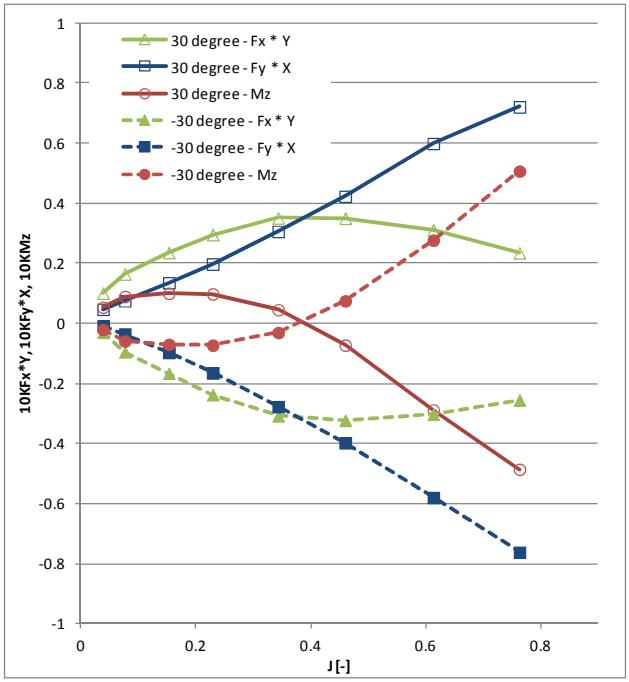

Figure 14: analysis of steering torque components based on equation (7): total steering torque in red, thrust eccentricity in green, side-force in blue. The positive steering angle is shown with solid lines and the negative steering angle with dotted lines.

5.3 Other contributors to steering torque

The analysis of the hydrodynamic steering torque has been discussed. It has to be noted that there are other factors affecting the final required steering torque of the steerable thruster unit. The torque from driveline will have an impact on the chosen steering direction as well as the inertia from the complete thruster unit. Finally the added mass of the unit will play a role in the dynamic steering effects.

CONCLUSIONS AND OUTLOOK

A very accurate performance prediction can be made with the presented RANS-CFD method. Good agreement with model scale experimental data has been found. The comparison of model scale and full scale CFD results showed a significant Reynolds scaling effect. The underlying phenomena have been explained, based on the approach of an axial pump. Maximum achievable bollard pull thrust for any generic thruster can be estimated, based on this approach. The validity of the T/P=0.18-IMCA rule has been shown to be limited for accurate full scale performance prediction.

The transient loads have been determined for many conditions, both with straight inflow and with oblique inflow. The amplitudes of propeller thrust and torque are below 10% for all cases. Steering with 30 degree at free sailing condition seems a more critical case.

The steering torque is a combination of both the thrust eccentricity on the unit and the side force on the nozzle. These two components are counterbalancing each other to a certain extend for moderate ship speeds and steering angles.

The behavior of a steerable thruster operating at oblique inflow is determined by the following parameters: inflow speed, steering angle and propeller RPM. Further analysis of the current results will be carried out in the near future to search for more trends.

ACKNOWLEDGEMENTS

The authors would like to thank Wärtsilä Propulsion CFD team for providing the numerical results presented in this paper and Marintek for the good cooperation when performing the model scale measurements.

REFERENCES

AMINI, H., SILEO, L., STEEN, S. (2012),'Numerical calculations of propeller shaft loads on azimuth Propulsors in oblique inflow', J Mar Sci Technol

BULTEN, N.W.H.(2006), 'Numerical analysis of the flow around a thruster', Dynamic Positioning Conference, Houston, USA

BULTEN, N.W.H. (2008), 'Determination of transient shaft forces in waterjets and thrusters based on CFD analyses', RINA Marine CFD conference, Southampton, UK

BULTEN, N.W.H., NIJLAND, M. (2011), 'On the development of a full-scale numerical towing tank', Second International Symposium on Marine Propulsors smp'11, Hamburg, Germany

IMCA M 140 rev 1 (2000), 'Specification for DP capability plots'

ITTC (1978), 15th ITTC'78 performance Prediction Method

OPREA, I., BULTEN, N.W.H. (2011), 'Analysis of the cavitating flow in a tunnel thruster', RINA Marine CFD conference, London, UK

PFLEIDERER, C. (1961), 'Kreiselpumpen', 5th ed. Springer Verlag